

Components of the Creep Strength of Welds

M. Murugananth and H.K.D.H. Bhadeshia
Department of Material Science and Metallurgy,
University of Cambridge, Pembroke street,
Cambridge CB2 3QZ, U. K. <http://www.msm.cam.ac.uk>

ABSTRACT

Modern power plant steels and welding alloys, designed to resist creep deformation at high temperatures, contain a myriad of alloying elements and a microstructure which has six or more phases. It has not therefore been possible to identify the precise role of each chemical and microstructural component in determining the ultimate creep properties.

In this work, we have used a combination of models and a knowledge of the mechanical properties and microstructure, to factorise the long-term creep rupture strength into individual contributions, for example due to solution strengthening, precipitate strengthening *etc.* The factorisation is non-linear and relies on thermodynamic and mechanical property models. The work is generic in the sense that it covers all common ferritic steels and welding alloys of the type used in the construction of power plant.

An assessment is included of some of the most modern alloys with interesting conclusions on the factors making major contributions to the long-term creep rupture strength.

INTRODUCTION

Ferritic steels are used extensively in the construction of power plant for the generation of electricity [1, 2, 3, 4, 5, 6, 7]. There are some intrinsic properties of ferrite which makes it suitable for high-temperature applications; thus, ferrite has a low thermal expansion coefficient and a high thermal conductivity when compared with austenite. Nickel alloys do have a sufficiently low expansion coefficient, but are expensive.

The main design requirement is that the ferritic steel should resist creep and oxidation, but should at the same time be easy to fabricate into very large components. This in turn means that they should be weldable and that any welds must be sufficiently robust to meet the creep requirements. There are in this context,

major international research programmes with the aim of designing novel steels and welding alloys [1, 2, 3, 4, 5, 6, 7]. The design procedure is based on scientific and engineering experience and the use of a variety of models, for example, phase stability calculations, the assessment of diffusion coefficients, kinetic theory associated with precipitation reactions, elementary creep theory and complex neural network models to express the creep strength as a function of a very large number of variables.

Elementary creep theory, such as that used in the construction of Ashby diagrams, is useful in gaining insight into the creep mechanisms, but is unable to predict the creep behaviour of multicomponent steels as a function of the chemical composition, heat treatment and service conditions. Neural network models based on vast experimental datasets are able to cope with such complexity and help visualise the nature of the interactions between variables in a way that is impossible with any other method of pattern recognition. They are, nevertheless, empiricals making it difficult to extract physical mechanisms.

The creep resistance of ferritic steels, over long periods of time at elevated temperatures, relies on the presence of stable precipitates which interfere with the climb and glide of dislocations, and which retard the coarsening rate of the microstructure as a whole, for example, the size and shape of martensite or bainite plates. The nature of the precipitate clearly depends on the detailed composition and heat treatment, but the variety is impressive, including Fe_3C (cementite), M_{23}C_6 , M_7C_3 , M_6C , M_2X , M_3C , Laves, M_5C_2 and Z-phase. There may typically be five or more of these precipitate phases in a creep-resistant steel.

Precipitation also affects the solute left in solution in the ferrite; solution strengthening is believed to be an important component of the long-term creep life. It would be incredibly useful to know quantitatively, the contribution made by each of the precipitate phases, and by solution strengthening due to each solute, to the long-term creep strength. There are currently no models capable either of extracting this information from experimental data or of making quantitative predictions. The purpose of the present work was to attempt precisely this task, using a neural network model but with inputs chosen to represent precipitates and solutes.

The work described here is based on steel plates rather than weld deposits. It has been demonstrated in previous work that as far as the creep-rupture life is concerned, there is no essential difference between weld metal and wrought metal [8].

SELECTION OF INPUTS

The neural network analysis published by Cole *et al.* [8] was based on an experimental database collected from the published literature, consisting of a total

of 5420 measurements with 37 variables, twenty of which represented the chemical composition and the remainder, the heat treatments, creep-rupture time and service temperature (tables 1, 2). They were able to accumulate such a large database with this particular choice of variables, because this is the form in which most experimental data are recorded. Our aim, on the other hand, was to discover the effects of precipitates and dissolved elements, both of which are impossible to find in reported data, certainly not from a quantitative perspective.

Therefore, a different approach is necessary, where the characteristics of precipitates and solutes are calculated from the Cole *et al.* data, and used as additional inputs to a neural network model. The characteristics necessary ideally include the precipitate volume fraction, size, location and number density. Whereas kinetic theory exists to attempt a prediction of the volume fraction, the other three quantities cannot be estimated in general. Therefore, it was decided that the focus should be on the very long-term creep rupture life, where the microstructure may be closest to equilibrium. In these circumstances, phase stability calculations using computer programs such as MTDATA [9] can be used to estimate the fractions of precipitates (and the composition of the ferrite matrix), data which serve as inputs to a neural network. From now on the phrase “precipitate fractions” refers to “equilibrium precipitate fractions”.

To summarise, the present work applies only to long-term creep, where the microstructure is likely to be close to equilibrium. Although the model produced is able to make calculations for short times, those calculations cannot be assumed to be valid since the precipitation may be evolving. As a rule, all the predictions illustrated in this paper are therefore for 100,000 h.

PHASE STABILITY CALCULATIONS

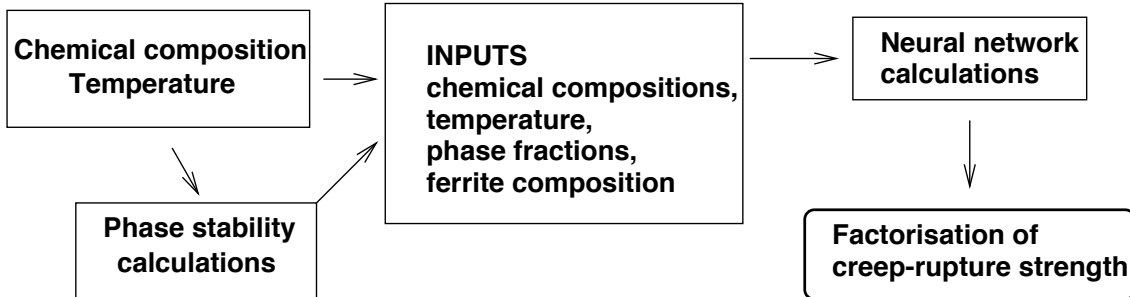
The equilibrium mole fractions of precipitates were calculated using MTDATA [9] which is a computer program which accesses the SGTE thermodynamic database. Given a chemical composition and temperature, it becomes possible to estimate not only the equilibrium phase mixture but also the chemical composition of each phase. The set of components and phases which are taken into account must first be specified. In the present work, the components included C, Si, Mn, P, S, Cr, Mo, W, Ni, Cu, V, Nb, Al, N, B, Co, Ta, O and Re, and the phases allowed included M_2X , cementite, M_7C_3 , $M_{23}C_6$, M_6C , Laves phases, NbC, NbN, VN and ferrite to exist. Notice that Z-phase is not included simply because the appropriate thermodynamic data are not available.

Since there were some 5420 separate sets of experimental data included in the creep database, the MTDATA program was linked to the database using the *application module* with MTDATA serving a FORTRAN computer program which accesses also the creep database. The required phase fractions and compositions could therefore be generated automatically, rather than feeding them individually into MTDATA.

DATABASE AND MODEL CONSTRUCTION

The database consists of the precipitate fractions and solutes obtained from the phase stability calculations along with other variables specified earlier. The spread of the data for composition and heat treatment for 5420 experiments can be found elsewhere in [8], but for the precipitates and solutes, which are of importance here is presented in figs 1, 2. The minimum, maximum, mean and standard deviation of the data for these variables are listed in table 3. An optimum committee consisting of 14 models was used to make predictions. The maximum perceived noise level for this committee was found to be 0.016 ($\pm 1\sigma$). A comparison between the predicted and measured values is illustrated in fig. 3. The description of the neural network analysis can be found in greater detail elsewhere [10, 11, 12].

The procedure for the factorisation of the creep-rupture strength is illustrated in the flow chart below; it begins with the calculation of phase-fractions and compositions which together with the average composition and temperature are fed into the creep-rupture neural network model. The neural network model is then interrogated to study the influence of each parameter in order to factorise the strength. It



is emphasised that the set of inputs to the neural network are not necessarily independent. For example, the chromium concentration cannot be varied without at the same time influencing the $M_{23}C_6$ carbide. These dependencies were always taken

into account in creating the inputs. Note also that the factorisation is non-linear and does not assume any particular relationship between the total creep-rupture strength and its components. This is now illustrated with a couple of case studies.

CASE STUDY: $2\frac{1}{4}$ Cr1Mo Steel

The calculations presented here are for the $2\frac{1}{4}$ Cr1Mo steel described in table 4; the normalising temperature was 1343 K for 1 h followed by tempering at 1043 K for 1 h. In all cases the sample was assumed to have been cooled in air from the heat treatment temperature.

Fig. 4 shows the results for this alloy at 550 °C , 10^5 h creep-rupture time, as a function of its molybdenum concentration. It is interesting that within the shaded regions, the only parameter which varies significantly with the total molybdenum concentration is the amount of molybdenum in solution in the ferrite. Therefore, by comparing the dissolved molybdenum data in the shaded region with corresponding calculations of the creep-rupture strength in the lower half of the diagram it is possible to calculate the contribution of dissolved molybdenum to the creep-rupture strength at 550 °C and 10^5 h. This turns out to be $\Delta\sigma_{Mo_{ss}} = 22$ MPa/wt%.

Note that this is not the same as solid-solution strengthening as measured in ordinary tensile tests, but rather some complex mechanism by which dissolved molybdenum influences creep deformation. There is diffusion and dislocation climb involved in creep processes whereas tensile deformation involves essentially the glide of dislocations. It is expected that the effect of a solute on tensile and creep deformation should show some correlation but for the reasons described the effects will not be identical.

For the specific composition of $2\frac{1}{4}$ CrMo steel given in table 4, *i.e.* 0.96 wt% of total molybdenum and $Mo_{ss} = 0.32$ wt% of dissolved molybdenum, contribution of the latter to the creep-rupture strength is about 7 MPa. Similar calculations gave the contribution of dissolved molybdenum to the creep-rupture strength at 600 °C and 10^5 h to be 15 MPa/wt% (this compares with 22 MPa/wt% at 550 °C). Therefore, as expected, the creep-strengthening effect of a unit concentration of dissolved molybdenum decreases as the temperature increases. However, the actual contribution in the $2\frac{1}{4}$ CrMo steel considered does not decrease significantly because of the amount of molybdenum in solution increases. The results are summarised in table 5.

It was not possible to do the same kind of analysis for the effect of chromium because there was no domain in which the effect of dissolved chromium could be studied in isolation. However, it is clear from fig. 5 that even in ordinary tensile

deformation the effect of chromium in solid-solution becomes negligible at elevated temperatures as illustrated from the work of Leslie [13].

The effect of vanadium is particularly interesting as illustrated in fig. 6, bearing in mind that vanadium has a strong affinity for nitrogen. As the total vanadium concentration is increased beyond 0.005 wt%, V_{ss} does not change, neither does NbN, but the amount of VN increases at the expense of M_2X (Cr_2N). In spite of the latter, the creep-rupture strength increases indicating that VN is a better creep-strengthener than M_2X . It is legitimate therefore to attribute the increase in creep-strength (fig. 6) due to the addition of vanadium to vanadium alone. The contribution is of course, a complex term due to formation of VN, solution strengthening from V_{ss} and a loss due to Cr_2N dissolution, but the net effect in this alloy is a gain of 4.8 MPa at 550 °C and of 2 MPa at 600 °C.

The influence of precipitates on the creep-strength is in principle deduced as follows. The key elements to consider with respect to precipitation are chromium, molybdenum and vanadium. Vanadium can be ignored in this analysis because total effect of vanadium has been identified separately. The solid-solution strengthening effect of chromium has been shown to be negligible and therefore its entire contribution must be attributed to precipitate strengthening. Molybdenum does cause a solid-solution strengthening effect, but this has been quantified and therefore can be excluded from its contribution due to precipitation. Therefore the contribution due to precipitates resulting from Cr and Mo can be calculated as the increase in creep-rupture strength on adding $2\frac{1}{4}$ Cr and 1 Mo wt% to the Cr- and Mo-free alloy less the solid-solution strengthening due to Mo.

Fig. 7 illustrates the variety of contributions to the creep-rupture strength; the diameter of the pie-charts have been scaled to reflect the 10^5 h creep-rupture strength at the appropriate temperature. The term microstructure excludes the precipitation and is intended to refer to cell boundaries and lath boundaries. It is particularly noticeable that the role of precipitate strengthening as a proportion of the total strength decreases sharply as the temperature is increased. This is hardly surprising, given the smaller equilibrium fraction of precipitates at higher temperatures and their greater coarsening rates, information which is implicit in neural network analysis.

It is noteworthy that the degree of factorisation illustration in fig. 7 is far from complete. Ideally, it would be desirable to know the contributions from each of the variety of precipitates present in the microstructure. For example, it is commonly stated that in $2\frac{1}{4}Cr1Mo$ steels, it is the Mo_2C which is the most important precipitate to resist creep deformation. It has not been possible to prove this with the present

analysis because of the fraction of Mo_2C cannot be varied independently without altering all the other precipitates. We should not be disheartened with this negative conclusion because it proves that it is not even experimentally possible to obtain this information, other than by direct characterisation of precipitate–dislocation interactions.

CASE STUDY: NF616 Steel

NF616 is a high–chromium creep–resistant martensitic steel intended for service at temperatures of $600\text{ }^\circ\text{C}$. Its chemical composition is listed in table 7. The analysis presented here is when the alloy is normalised at 1343 K for 1 h followed by air cooling to ambient temperature, tempering at 1043 K for 1 h followed by air cooling. Notable features about NF616 include its tungsten and vanadium concentrations, and the presence of Laves phase in the microstructure.

Fig. 8 shows an interesting synergistic effect between tungsten and molybdenum in NF616, whereby the strengthening effect of V depends on the W concentration. It has been verified that this synergy cannot be explained on the basis of variations in the equilibrium phase–fractions or phase compositions. The reasons are not clear but it is speculated that they could be related to phenomena such as diffusion. In any event, the creep–rupture strength of the $0.2\text{V}–1.84\text{W}$ alloy is calculated to be 133 MPa whereas the removal of W gives the strength of $0.2\text{V}–0\text{W}$ to be 91 MPa . Therefore, the total contribution of W to the 10^5 h creep–rupture strength is $133 - 91 = 42\text{ MPa}$ (table 8). Given this value and fig. 8, and the creep–rupture strength for a $0\text{V}–1.84\text{W}$ (31 MPa) alloy and $0.2\text{V}–1.84\text{W}$ (133 MPa) alloy, the total contribution of V equals $133 - 42 - 31 = 60\text{ MPa}$ (table 8). The total effect of Mo was obtained similarly. There is no significant effect of niobium on the creep–rupture strength at $600\text{ }^\circ\text{C}$ (fig. 13). Another observation is that location of NF616 on the contour plot shown in fig. 14 indicates optimum design.

The contribution of vanadium can be further factorised because there is a regime of alloy composition where the vanadium in solid–solution, V_{ss} , varies independently of other variables (fig. 11). The results from this factorisation are also presented as contributions due to V_{ss} and VN in table 8. It is evident that VN plays a major role in the creep properties of NF616. Similarly, W_{ss} can be estimated using fig. 8 so that the contribution from Laves phase amounts to 25.3 MPa . This agrees qualitatively with claims in the literature that Laves phase makes an important contribution to the strength of NF616.

It is reasonable to assume that the contribution to the creep–rupture strength from iron and the microstructure should be similar to that of $2\frac{1}{4}\text{Cr}1\text{Mo}$ steel. The

pie-chart in fig. 15 gives summary of the contributions made by the different components of NF616 to its 10^5 h creep-rupture strength at 600 °C.

CONCLUSIONS

A combination of neural network models to predict the mechanical properties and phase stability calculations to identify the phases, were used in factorising the creep strength of the heat-resisting steels, $2\frac{1}{4}$ Cr1Mo and NF616. The factorisation was non-linear.

In the case of $2\frac{1}{4}$ Cr1Mo steels, the proportion of contribution to 10^5 h creep-rupture strength from dissolved solutes increased at 600 °C in comparison with 550 °C.

For the high chromium heat-resisting steel, NF616, vanadium nitride is a strong contributor to the creep-strength at 600 °C . In this tungsten alloyed steel Laves phase contributes more to the creep-strength than dissolved tungsten as expected [14]. The contribution from the inherent strength of iron along with the microstructure is comparatively less than from other components.

Input component	Minimum	Maximum	Mean	Standard Deviation
log (creep rupture time /h)	-1.7696	5.2847	3.0627	1.1104
Temperature (K)	723.0000	1023.0000	861.4081	65.1107
wt% of elements				
Carbon	0.0040	0.4800	0.1219	0.0560
Silicon	0.0100	0.8600	0.2678	0.1848
Manganese	0.0100	0.9200	0.5196	0.1087
Phosphorus	0.0010	0.0290	0.0126	0.0062
Sulphur	0.0005	0.0200	0.0076	0.0049
Chromium	0.5900	14.7200	6.5537	4.1291
Molybdenum	0.0400	2.9900	0.7236	0.4204
Tungsten	0.0100	3.9300	0.6427	0.8566
Nickel	0.0100	2.0000	0.1822	0.2296
Copper	0.0030	1.5600	0.1104	0.2231
Vanadium	0.0100	0.3000	0.1275	0.1035
Niobium	0.0010	0.3120	0.0294	0.0372
Aluminium	0.0010	0.1651	0.0280	0.0235
Nitrogen	0.0010	0.0570	0.0098	0.0097
Boron	0.0000	0.0510	0.0009	0.0029
Cobalt	0.0000	3.0900	0.0554	0.3257
Tantalum	0.0000	0.1000	0.0002	0.0045
Oxygen	0.0030	0.0350	0.0099	0.0020
Rhenium	0.0000	1.6900	0.0057	0.0807

Table 1: Service time and temperature along with chemical composition. See also table 2.

Input component	Minimum	Maximum	Mean	Standard Deviation
Normalising Temperature (K)	1123.0000	1473.0000	1268.5221	71.8127
Normalising Time (h)	0.1667	33.0000	2.4260	4.5454
Cooling rate of Normalise in furnace (0 or 1)	0.0000	1.0000	0.0423	0.2012
Cooling rate of Normalise in air (0 or 1)	0.0000	1.0000	0.7421	0.4375
Cooling rate of Normalise for oil quench (0 or 1)	0.0000	1.0000	0.1520	0.3591
Cooling rate of Normalise for water quench (0 or 1)	0.0000	1.0000	0.0637	0.2442
Tempering Temperature (K)	823.0000	1323.0000	998.8745	73.3174
Tempering time (h)	0.5000	83.5000	4.8076	11.2443
Cooling rate of Temper in furnace (0 or 1)	0.0000	1.0000	0.0559	0.2298
Cooling rate of Temper in air (0 or 1)	0.0000	1.0000	0.8996	0.3005
Cooling rate of Temper for oil quench (0 or 1)	0.0000	1.0000	0.0312	0.1738
Cooling rate of Temper for water quench (0 or 1)	0.0000	1.0000	0.0133	0.1145
Annealing temperature (K)	300.0000	1023.0000	461.5393	282.6159
Annealing Time (h)	0.5000	90.0000	4.3790	11.0136
Cooling rate of anneal in furnace (0 or 1)	0.0000	1.0000	0.1271	0.3331
Cooling rate of anneal in air (0 or 1)	0.0000	1.0000	0.8729	0.3331

Table 2: Heat treatment parameters.

Input component	Minimum	Maximum	Mean	Standard Deviation
All units in mole fraction				
M ₂ X	0	0.9857	0.0034	0.0436
Cementite	0	0.0397	0.0002	0.0026
M ₇ C ₃	0	0.0407	0.0013	0.0055
M ₂₃ C ₆	0	0.0554	0.0235	0.0099
M ₆ C	0	0.0134	0.0006	0.002
Laves phases	0	0.0317	0.0037	0.0056
Niobium carbide	0	0.0031	0	0.0002
Niobium nitride	0	0.0038	0.0003	0.0004
Vanadium nitride	0	0.0049	0.0015	0.0015
wt% of solid solution strengthening elements				
Chromium	0.0009	13.0613	5.2916	3.7615
Molybdenum	0.003	2.7086	0.274	0.3038
Tungsten	0	1.6607	0.2647	0.3963
Vanadium	0	0.2154	0.0422	0.0549
Niobium	0	0.0009	0.0001	0.0002
Nitrogen	0	0.0141	0.0003	0.0013
Carbon	0	0.0061	0.0003	0.0006
Output variable				
Creep strength / MPa	18.0	568.9		
log(Creep strength / MPa)	1.255	2.755100	2.1447	0.2825

Table 3: Equilibrium precipitate fractions and wt% solid solution strengthening elements used as inputs. The output is stated in the last two rows, both as creep-rupture strength and its logarithm; only the latter is used in the development of the model, the former is simply there for illustration.

C	Si	Mn	P	S	Cr	Mo	W	Ni	Cu
0.12	0.29	0.5	0.018	0.018	2.25	0.96	0.01	0.027	0.05
V	Nb	N	Al	B	Co	Ta	O	Re	
0.01	0.005	0.0099	0.004	0	0.05	0	0.01	0	

Table 4: Composition (wt%) of 2 $\frac{1}{4}$ Cr1Mo steel

Temperature / °C	$\Delta\sigma_{Mo_{ss}}$ / MPa wt% ⁻¹	Mo _{ss} / wt%	$\Delta\sigma_{Mo_{ss}} \times Mo_{ss}$ / MPa
550	22	0.32	7.0
600	15	0.43	6.3

Table 5: Summary of the effect of molybdenum dissolved in ferrite on the 10⁵ h creep-rupture strength of 2 $\frac{1}{4}$ Cr1Mo steel.

Components	Strength Contribution / MPa	
	550 °C	600 °C
Molybdenum in solid solution	6.97	6.32
Total Vanadium	4.78	2.07
Precipitates	17.78	3.21
Fe, microstructure and other SSS	49.08	18.89
Total strength at temperature	78.69	30.49

Table 6: Strength contribution from different components of $2\frac{1}{4}$ CrMo steel.

All elements in wt%									
C	Si	Mn	P	S	Cr	Mo	W	Ni	Cu
0.106	0.04	0.46	0.008	0.001	8.96	0.47	1.87	0.06	0
V	Nb	N	Al	B	Co	Ta	O	Re	
0.2	0.069	0.051	0.007	0.001	0.015	0	0.01	0	

Table 7: Composition of NF616.

	Strength / MPa
Creep Rupture Strength	133.0
Fe + microstructure + 1_{ss}	18.9
Total from tungsten	42.0
Total from vanadium	60.0
Total from molybdenum	12.0
Total from V_{ss}	13.0
Total from VN	47.0
Total from W_{ss}	16.7
Total from Laves phase	25.3

Table 8:

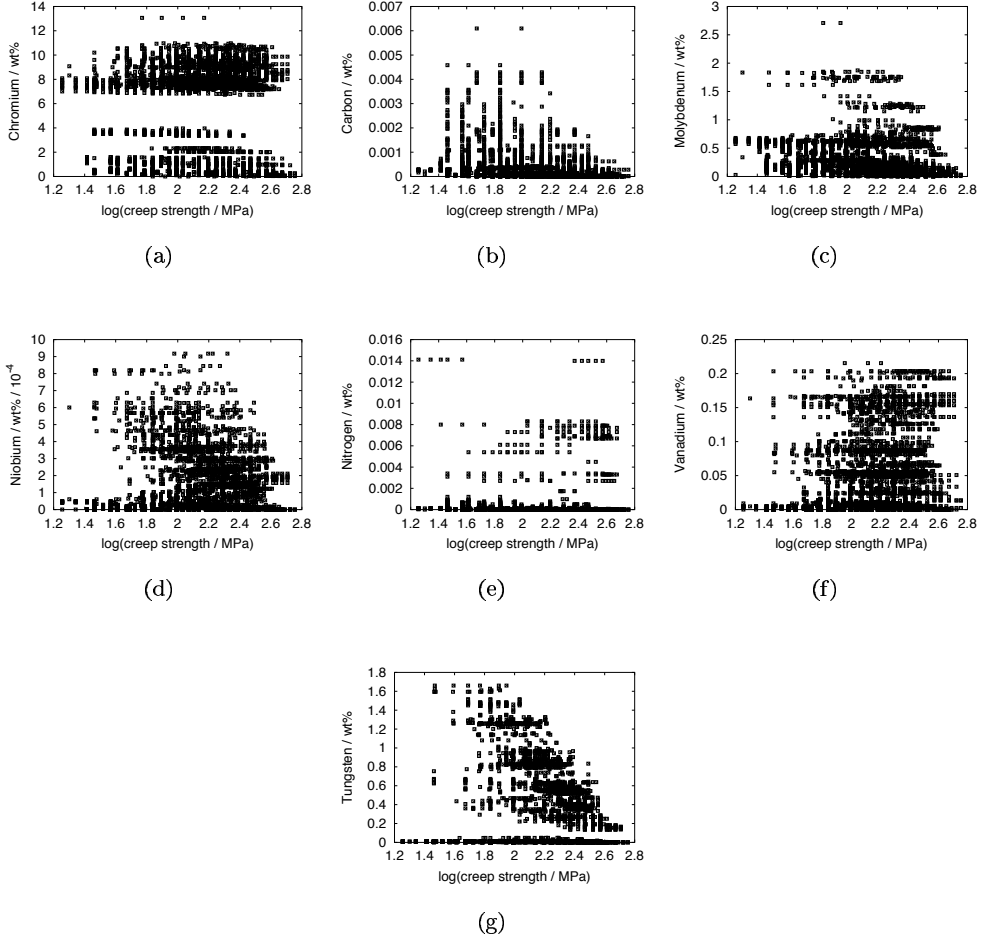


Figure 1: Spread of wt% of solid solution strengthening solutes.

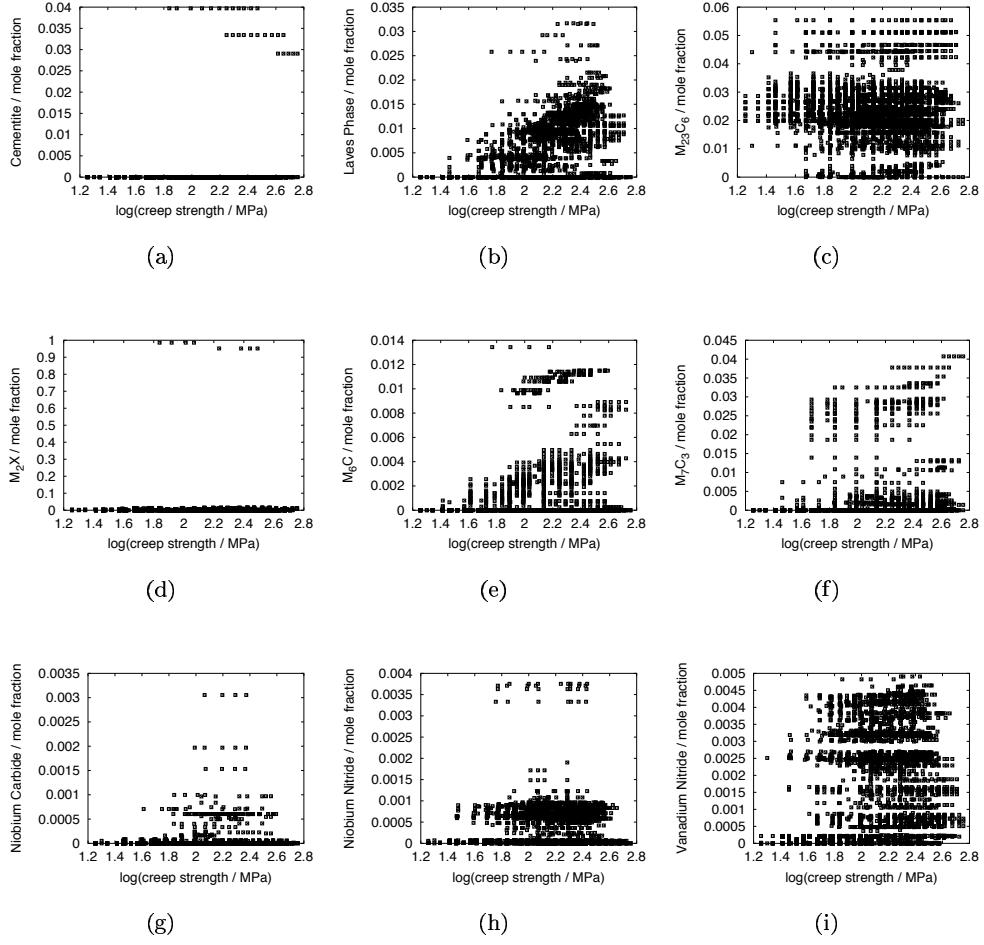
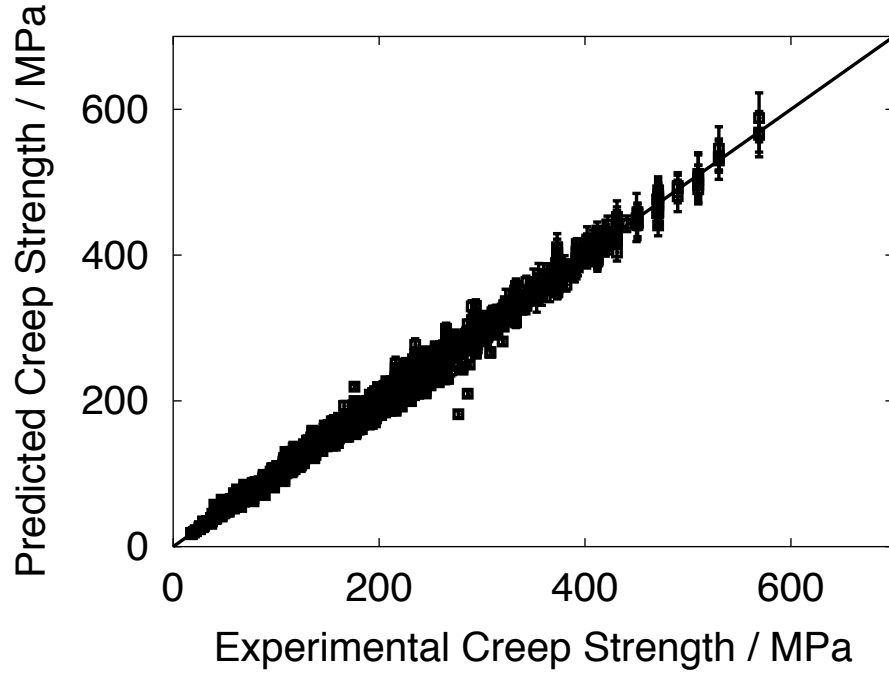
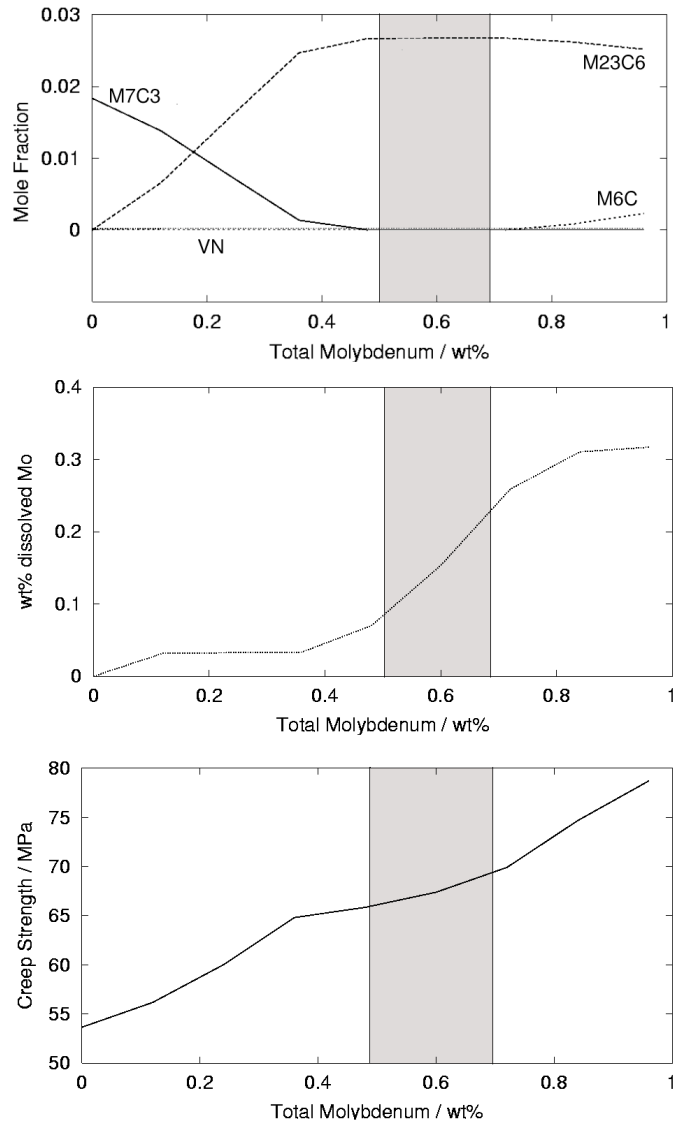


Figure 2: Spread of precipitate mole fraction.



(a)

Figure 3: Comparison between the calculated and measured creep-rupture strength for 5420 separate experiments. The calculations were done using the complete dataset following a retraining procedure once the appropriate set of models which form the committee were selected as described in [8].



(a)

Figure 4: The shaded regions represent total molybdenum concentrations where only the amount of molybdenum in solution is changing significantly. The calculations are for $2\frac{1}{4}\text{CrMo}$ steel at $550\text{ }^{\circ}\text{C}$ for creep-rupture time of 10^5 h .

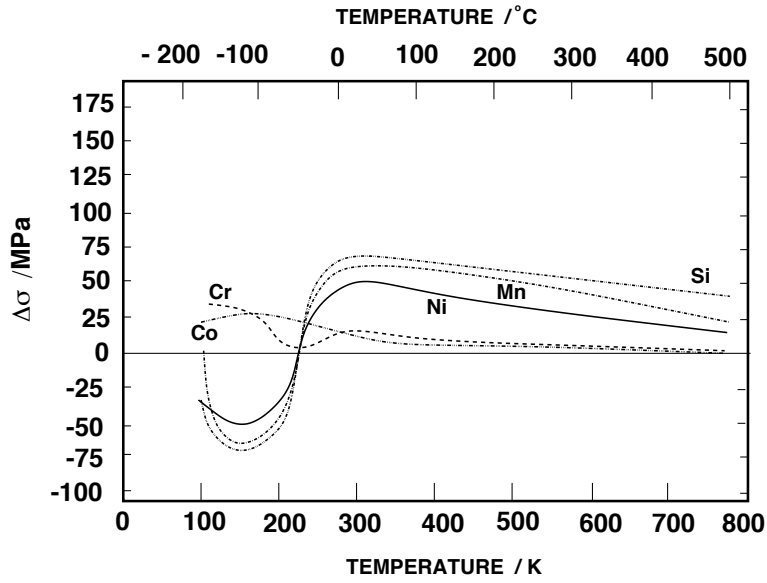


Figure 5: Solid-solution hardening and softening in iron-base alloys, adapted from Leslie [13]

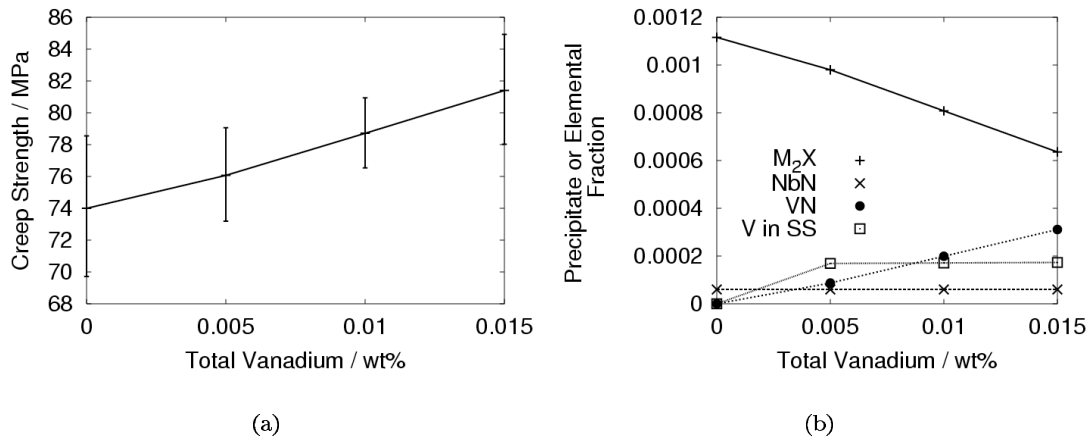


Figure 6: Precipitate fractions, and creep strength, as a function of total vanadium concentration, of $2\frac{1}{4}$ Cr1Mo steel for a creep-rupture time of 10^5 h at 550 °C.

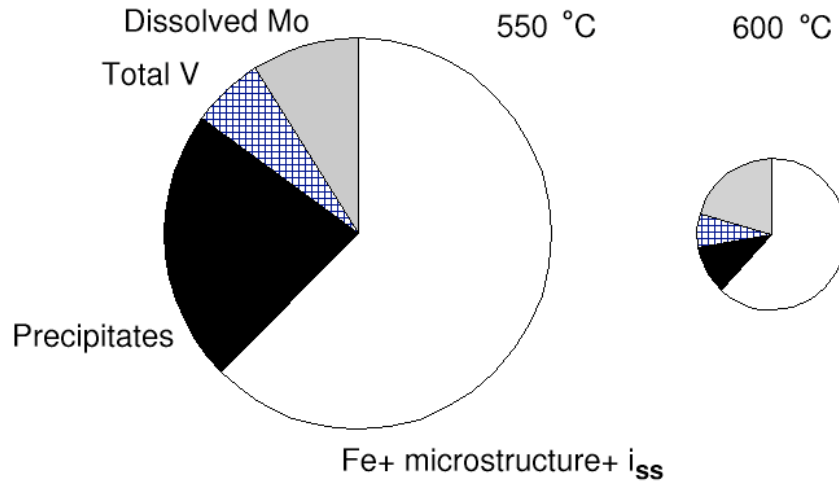


Figure 7: Pie charts showing the factorisation of the 10^5 h creep-strength of $2\frac{1}{4}$ CrMo. The diameters of the pie charts have been scaled to reflect the 10^5 h creep-rupture strength at the appropriate temperature. The term i_{ss} represents the contributions to the creep-rupture strength due to dissolved solutes other than molybdenum and vanadium.

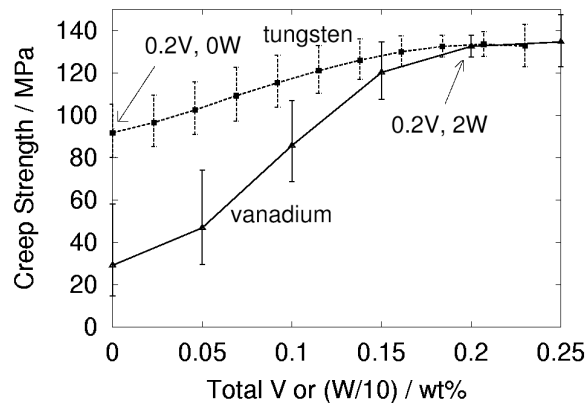


Figure 8: Synergistic effect of tungsten and vanadium on the creep-rupture strength of NF616.

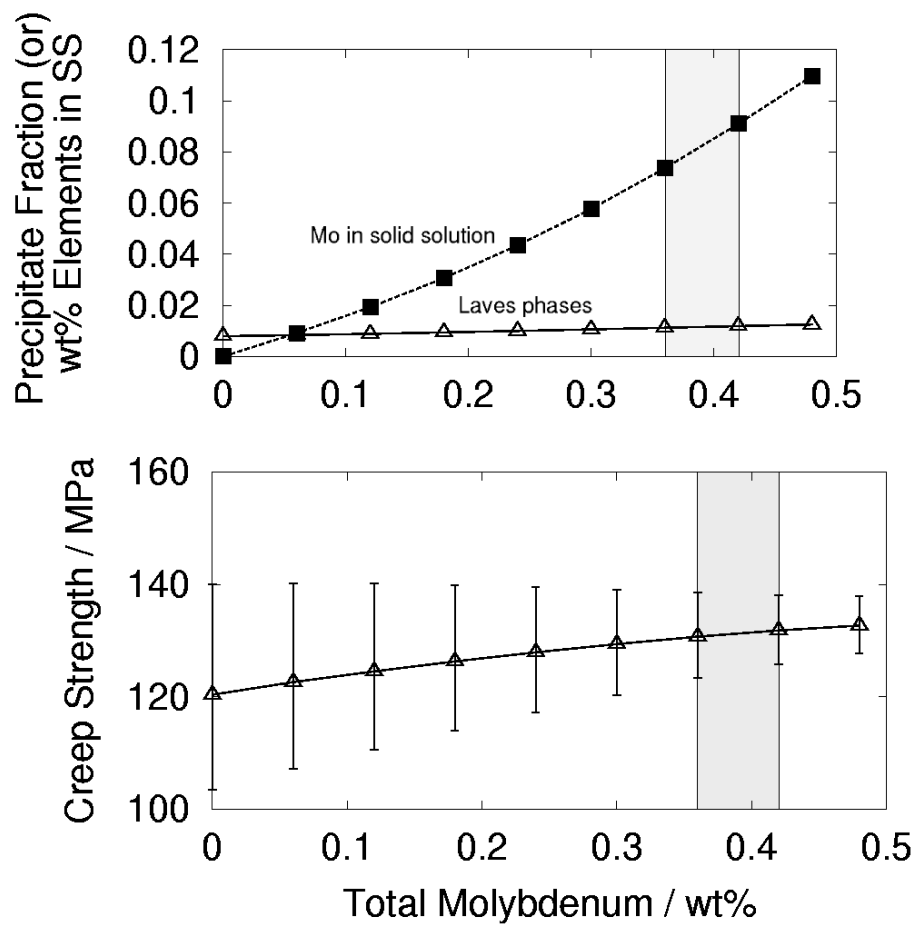


Figure 9: Precipitate fractions, and 10^5 h creep strength of NF616 at 600 °C.

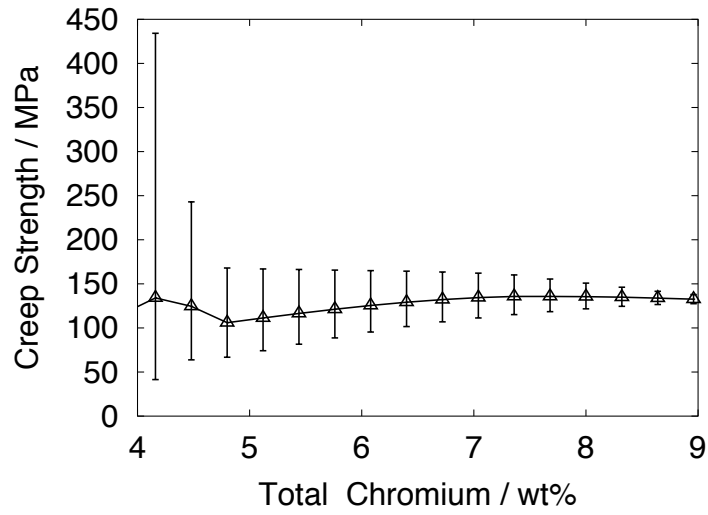


Figure 10: 10^5 creep-rupture strength is not significantly influenced by the presence of chromium at 600 °C.

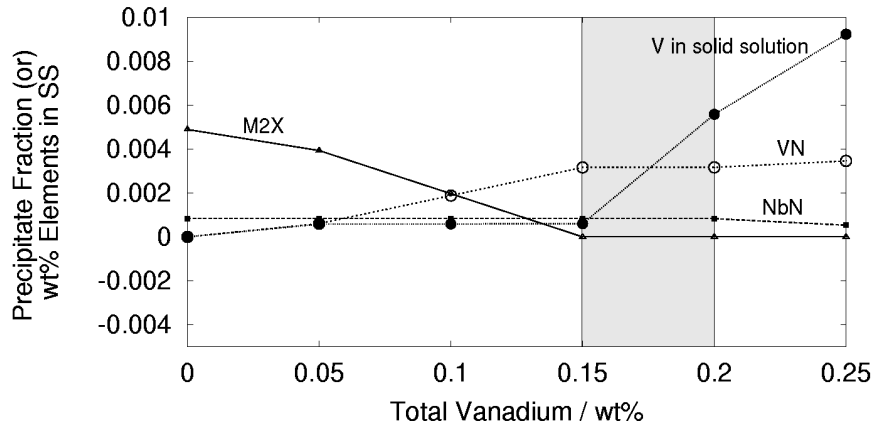


Figure 11: Precipitate fractions and wt% of vanadium in solid solution of NF616 at 600 °C. Note that over the concentration range 0.15–0.2 wt% it is only the amount of vanadium in solution that varies significantly. This domain can therefore be used to estimate $\Delta\sigma_{ss}^V$.

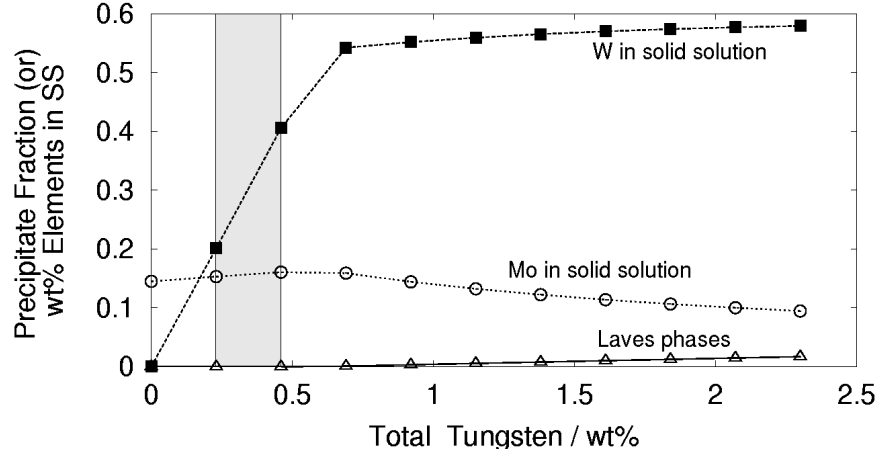


Figure 12: Precipitate fractions, and creep strength of NF616 after 10^5 h at 600 °C. Note that over the concentration range 0–0.5 wt% it is only the amount of tungsten in solution that varies significantly. This domain can therefore be used to estimate $\Delta\sigma_{ss}^W$.

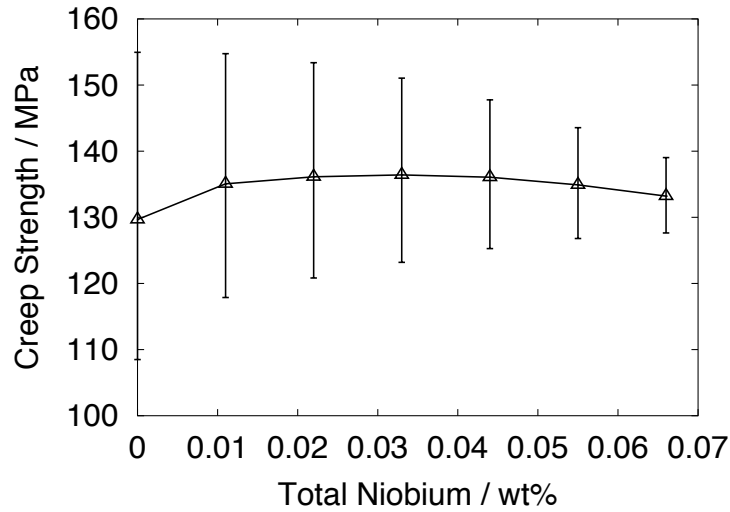


Figure 13: Precipitate fractions, and creep strength of NF616 after 10^5 h at 600 °C.

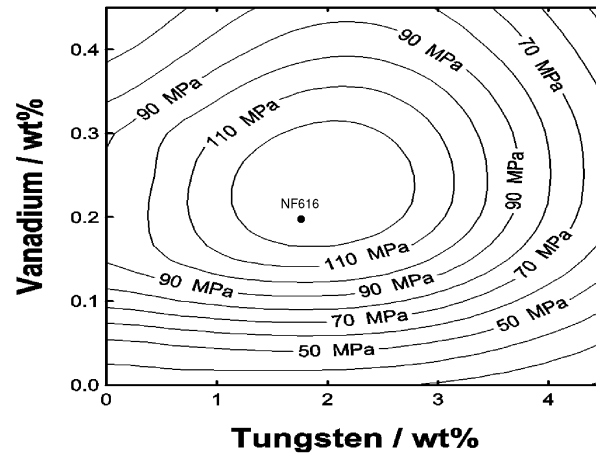


Figure 14: Contour plot showing the variation in creep-rupture strength at 600 °C, when concentrations of both vanadium and tungsten are varied simultaneously. Note that the domain where NF616 is present is optimum.

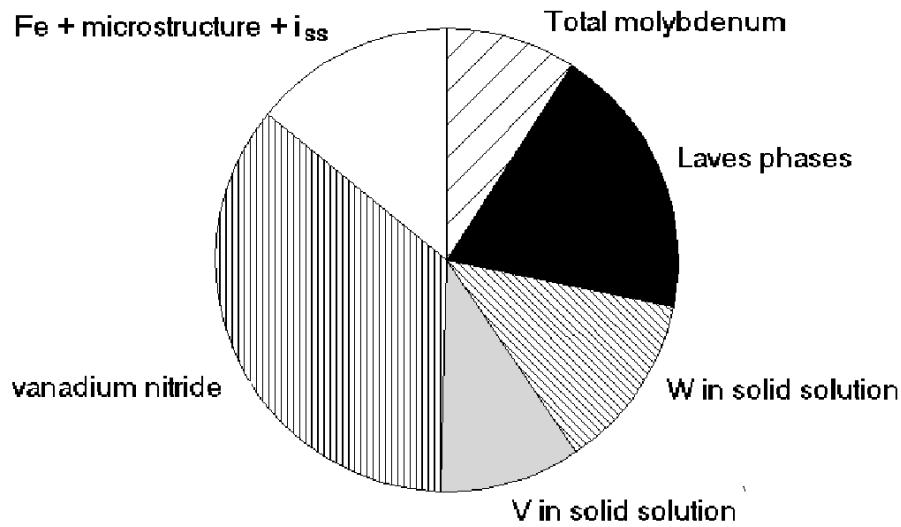


Figure 15: Pie charts showing the factorisation of the 10^5 h creep-strength of NF616. The term i_{ss} represents the contributions to the creep-rupture strength due to dissolved solutes other than molybdenum, vanadium and tungsten.

Bibliography

- [1] F Abe, M Igarashi, N Fujitsuna, K Kimura, and S Muneki. In Lecomte-Beckers *et al.*, editor, *6th Leige Conference on Materials for Advance Power Engineering*, pages 259–268, October 1998.
- [2] Cerjak Horst, Hofer Peter, and Schaffernak Bernhard. *ISIJ International*, 39(9):874–888, 1999.
- [3] H. K. D. H Bhadeshia. *ISIJ International*, 41(6):626–640, 2001.
- [4] F. Masuyama. *ISIJ International*, 41(6):612–625, 2001.
- [5] K. Maruyama, K. Sawada, and J. Koike. *ISIJ International*, 41(6):641–653, 2001.
- [6] T Fujita. In E. Metcalfe, editor, *New steels for Advanced plant upto 620 °C*, pages 190–200, 58, Abingdon Road, Drayton, Oxon, OX14 4HP, UK, May 1995. National Power, PicA.
- [7] T Fujita. *Metal Progress*, 130:33–36, 1986.
- [8] D. Cole, C. Martin-Moran, A. G. Sheard, H. K. D. H. Bhadeshia, and D. J. C. MacKay. *Science and technology of welding and joining*, 5:81–90, 2000.
- [9] S. M. Hodson. MTDATA - Metallurgical and Thermochemical Databank. National Physical Laboratory, Teddington, U.K., 1989.
- [10] D. J. C. MacKay. *Neural Computation*, 4:448–472, 1992.
- [11] H. K. D. H. Bhadeshia, D. J. C. MacKay, and L. E. Svensson. *Mater. Sci. Technol.*, volume 11:1046, 1995.
- [12] David MacKay. In H Cerjak, editor, *Mathematical Modelling of Weld Phenomena*, 3, pages 359–389. Institute of Materials, 1997.

- [13] W. C. Leslie. *The physical metallurgy of steels*. McGraw-Hill, London, 1981.
- [14] J Hald. In E. Metcalfe, editor, *New steels for Advanced plant upto 620 °C*, pages 152–173, 58, Abingdon Road, Drayton, Oxon, OX14 4HP, UK, May 1995. National Power, PicA.